# Chapter 1

## 1.1 Perovskites

Gustav Rose discovered the mineral calcium titanium oxide ($CaTiO_3$) in the Russia's Ural mountains in 1839 and named as perovskite on the name of Russian mineralogist Lev Perovski.. Perovskite is found material having the same crystal structure as $CaTiO_3$. Pervoskite is represented by general chemical formula $ABO_3$ where A and B are used for two cations having different size. The 'A' atom is bigger than the 'B' one. In the case of ideal cubic structure, B cation has the 6-fold and A cation has 12-fold cuboctahedral coordination and B cation is surrounded by an octahedron made by anions [1, 2]. The ions in the *Pm*3 *m* space group for the perovskite oxide occupy the Wyckoff positions as "A" at (0, 0, 0), "B" at (1/2,1/2,1/2) and "O" at (0, 1/2,1/2). In the ideal cubic perovskite structure, A and B ions are located at the center of cuboctahedron (dodecahedral site) and octahedron formed by the O ions, i.e., $AO_{12}$ and $BO_6$, respectively. The schematic illustration of the cubic perovskite structure is given in **figure 1.1**. In 1926, Goldschmidt defined a new parameter denoted by "t" and now is well known as structural tolerance factor or simply tolerance factor, to predict the stability (deformability from the ideal cubic structure) of the perovskite structure [3]. The expression for the estimation of tolerance factor t, associated with the ionic radii, is obtained by using the concept of well known closed packed theory of ions. The ionic radii of A, B and O atoms under appropriate coordination environment are represented as $r_A$, $r_B$ and $r_O$ , respectively. In the case of a stable perovskite structure, the t lies in the range of $0.88 < t < 1.05$. For $t = 1$, the perovskite structure is anticipated to adopt the ideal cubic symmetry (*Pm3m* space group).

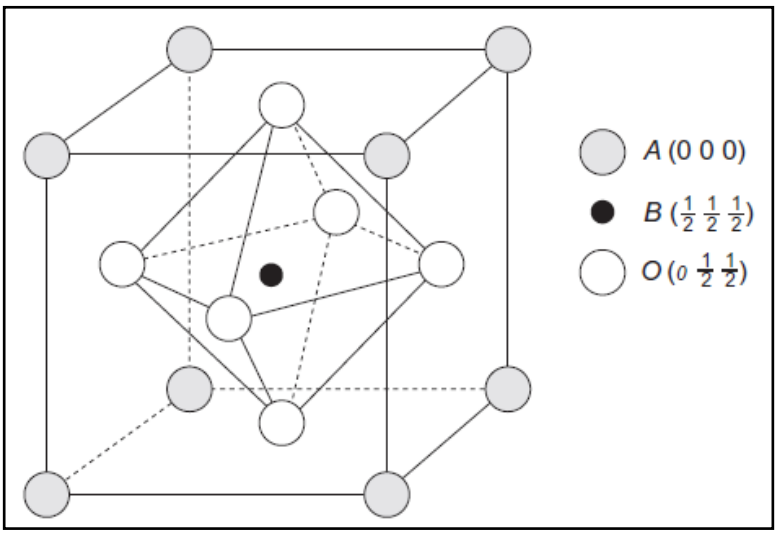


***Figure 1.1*** *Crystal structure of perovskite $ABO_3$.*

In the case of t > 1, the B atom is so small for $BO_6$ (the oxygen octahedron) so that the structure will build up a small polar distortion in the structure, as appears in $BaTiO_3$. However, when t < 1, the A atom is small for the oxygen cuboctahedral coordination ($AO_{12}$) and cannot effectively bond with all twelve adjoining O atoms. When the value of t is only slightly less than one, then the tilting and rotations of the oxygen octahedra ($BO_6$) will be favored as is the case with $CaTiO_3$.

## 1.2 Structure of Pervoskite: Rare Earth Manganite

One of the important perovskite compound is $RMnO_3$ rare earth manganites, where R represents rare earth metal possess perovskite structure. The history of the manganites belongs to 1950 [4, 5] when Jonker and van Santen have carried out early work on the compound $La_{1-x}A'_xMnO_3$ with A'=Ca, Sr, and Ba. The ideal perovskite rare earth manganites occur in cubic symmetry when the $MnO_6$ octahedra is undistorted. When A site

is doped with dopant having different ionic radii or B site cation is replaced by other dopant a change in value of t arises. Due to changet in value of t, cubic symmetry is converted to tetragonal or orthorhombic structure. As a result of this, lattice distortion and octahedral tilting occurs which alter the structural and physical properties of the compounds. Such modifications are strongly coupled with their intrinsic Jahn-Teller (J-T) distortion. J-T distortion is decided dependency on d-orbitals according to crystal field splitting. Usually in manganites J–T distortion is found. The physical properties of the manganites are depend strongly on inherent structural imperfections.

### 1.2.1 Crystal Field

The crystal field is an electric field resulting from neighboring atoms of the crystal. According to crystal field theory (CFT) the neighboring orbitals are modeled as the negative point charges. The advanced systematic work on this approximation is ligand field theory which essentially expands the molecular orbitals theory revealing crucial character of d orbitals on the central cation which overlap with nearby orbitals adjacent anions (ligands). The nature and size of the crystal field effects significantly depend on the local environment symmetry. There are two types of environments present one is octahedral and another one is tetrahedral. For example in several transition metal compound, the octahedron is made when the oxygen sit on each corner of it with central metal ion. In this case the crystal field arises due to electrostatic repulsion which originates from the oxygen orbitals filled with negatively charged electrons. So, mainly CFT is used to describe the breaking of degeneracy of the electronic orbital states. The five d orbitals commonly designated as $d_{xy}$, $d_{yz}$, $d_{zx}$, $d_{z2}$ and $d_{x2-y2}$ (**figure 1.2**) split based on the symmetry of the electrostatic field produced by particular lattice site anions. The d orbitals categorized into

two classes one is $t_{2g}$ in which orbitals are pointed between the x,y and z axes i.e, $d_{xy}$, $d_{zx}$ *and* $d_{yz}$ orbitals and $d_{z2}$ and $d_{x2-y2}$ orbitals belong to $e_g$ in which the they are along the axes. In an octahedral field, a lower triplet formed by orbitals $d_{xy}$, $d_{yz}$ and $d_{zx}$ i.e, $t_{2g}$ and a higher doublet with orbitals $d_{z2}$ and $d_{x2-y2}$ i.e, $e_g$ because of these orbitals point directly to the anions [6]. In **figure 1.3**, Δ denotes the difference in energy between the triplet ($t_{2g}$) and the doublet ($e_g$) states. The energy $t_{2g}$ is stabilized by amount -0.4 Δ and $e_g$ level is destabilized by + 0.6 Δ (+ve sign is used for increase in energy, -ve sign for decrease in energy). The central compounds to this thesis having perovskite crystal structure, with a central $Mn^{3+}$ ion which is surrounded by an octahedron made of $O^{2-}$ ions. Electrostatic forces occur in this case between Mn ion's d orbital and the oxygen ion's p orbitals.

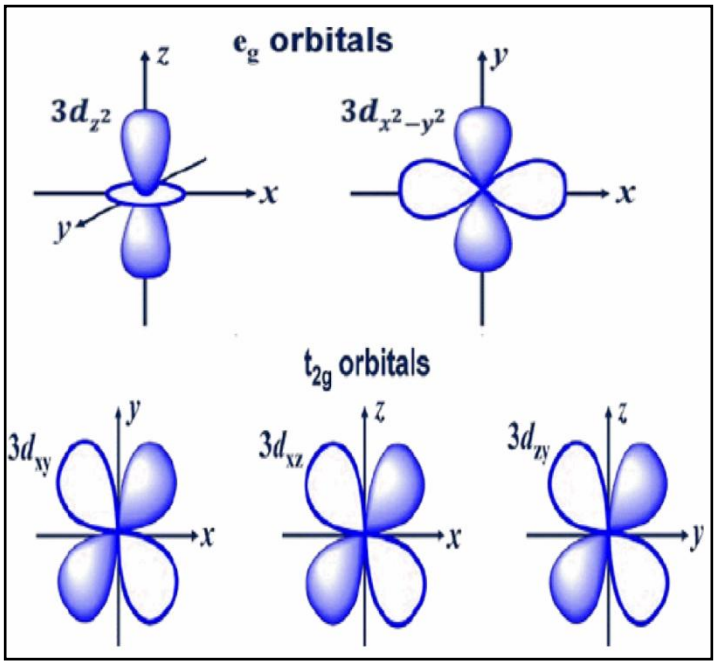


***Figure 1.2*** *Representation of the d orbitals.*

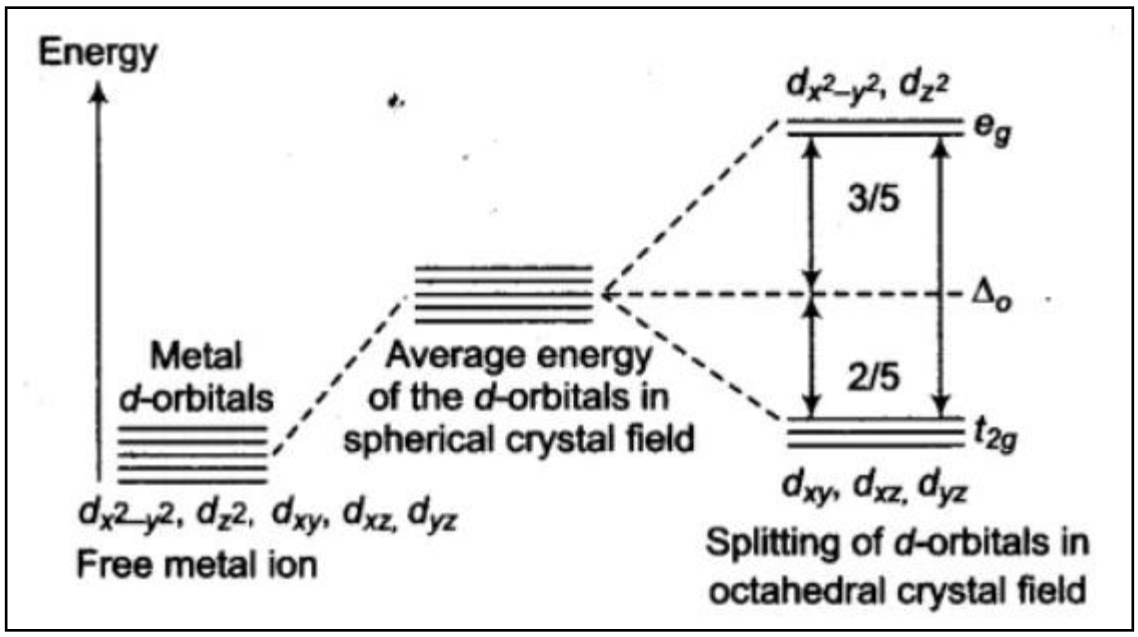


***Figure 1.3*** *d orbitals splitting in octahedral crystal field in perovskite.*

The d orbitals, in the $Mn^{3+}$ ($3d^4$) ions, are divided into five different forms: one is $e_g$ levels ($d_z^2$ and $d_{x^2-y^2}$), in which the orbitals are pointed along the axes x, y and z; and the other one is $t_{2g}$ levels ($d_{xy}$, $d_{xz}$ and $d_{yz}$) in which orbitals are pointed between the axes. The p orbital having three types, $p_x$, $p_y$ and $p_z$, which are pointed along their respective axis. Therefore, in the case of octahedral environment the $e_g$ orbitals have high energy configuration in comparison to the $t_{2g}$ orbitals. The splitting of energy levels of d orbitals are shown in **figure 1.3**. The amount of splitting, Δ is dependent on such factors such as the the repulsion between the ions, geometry of the octahedra and the effects of Jahn-Teller distortion.

### 1.2.2 Jahn –Teller Distortion

As discussed in the earlier paragraph, the splitting of an $e_g$ doublet and a $t_{2g}$ triplet occurs because of crystal-field effect. In the case of $Mn^{3+}$ ($t_{2g}^3$ $e_g^1$) ion, the presence of the

doubly degenerate $e_g$ levels, the octahedron is distorted to remove the degeneracy of the levels (**figure 1.4**).

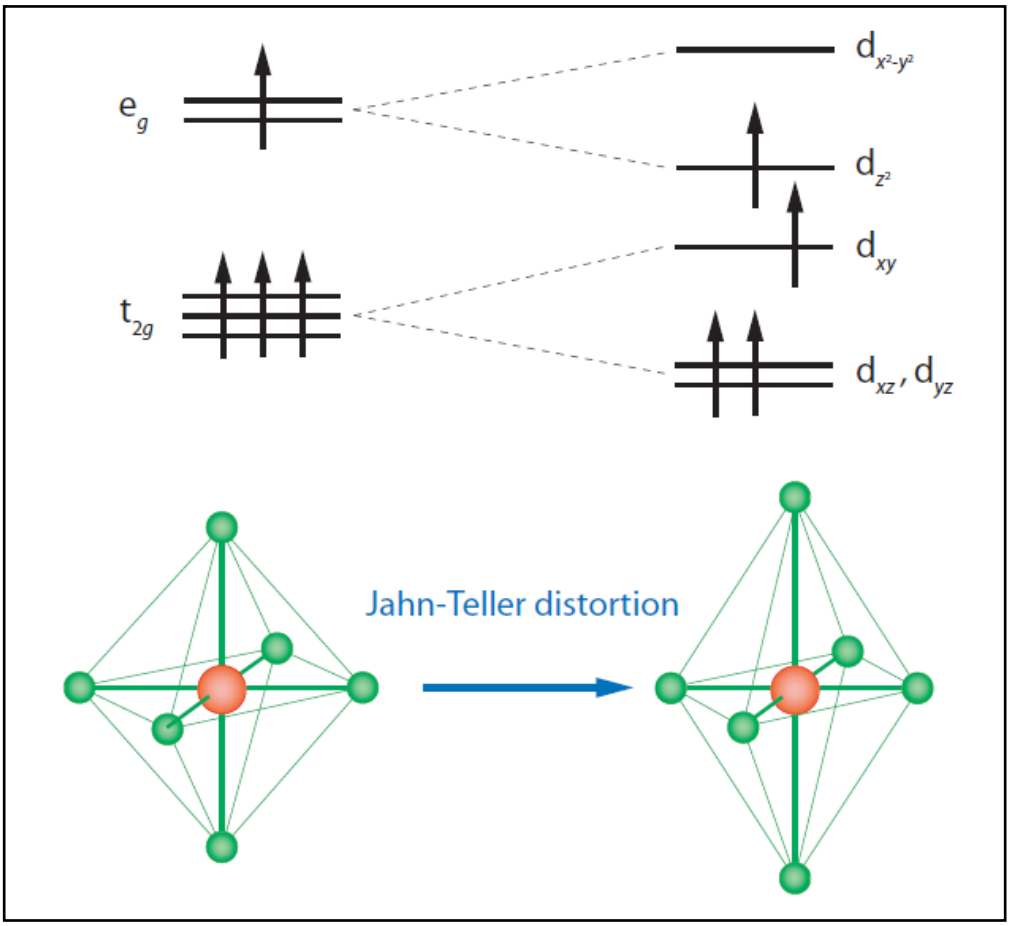


***Figure 1.4*** *Jahn-Teller distortion in $Mn^{3+}$ ions in rare earth manganites [6].*

To remove the degeneracy, the O ions which are around the $Mn^{3+}$ ions readjust their location to create an asymmetry in different directions. The elimination of degeneracy because of orbital lattice effect is known as co-operative J-T effect [7]. This effect tends to occur because it is energetically favorable to spontaneously distort the lattice, thus removing the degeneracy. The octahedron $MnO_6$ is distorted as that there are long and short Mn-O bonds appeared. This is usually manifested in the form of a basal plane

distortion with one diagonally opposite oxygen pair displaced outwards and the other pairs displaced inwards. Moreover, the J-T distortion can both be static and dynamic. The static J-T distortion occur in manganite with small hole density while the dynamic J-T distortion occurs when the ion is not frozen in one distorted configuration but evolve among several configuration as a function of time. The magnetic properties of manganites are strongly corelated to J-T distortion.

## 1.3 Magnetism

Following the elementary investigations of quantum mechanics, the magnetism emerges primarily due to the electron spin and their exchange interactions. In recent days, the deeper thoughtful of magnetic properties permit us to use the magnets in form of advance devices in regular life. The emerging area, where magnetic behavior of manganites being explored is spintronics, switching, potential applications and so on.

### 1.3.1 Fundamental Theory of Magnetism

The source of magnetism is the behavior of electrons in atoms. There are two types magnetic moment that contribute independently to the overall magnetism of a material - orbital magnetic moment and intrinsic spin moment of electrons. Thus, all atoms with a minimum of one electron show some sort of magnetism, even though, the useful magnetic behavior is observable only in molecules and atoms consisting of unpaired electrons. This is due to Pauli's exclusion principle which states that an orbital can have a maximum of only two electrons with anti-parallel spins, which effectively cancel magnetic moment of one another. The transition metals such as manganese, cobalt, nickel and iron which possess unpaired d-electrons are most common examples of magnetic materials where spontaneous magnetization is observed. The magnetic behavior of these elements arises

mainly due to exchange interaction between the electrons. The rare earth elements due to unpaired f-electrons including elements like gadolinium, neodymium, europium, samarium and cerium also exhibit magnetic properties. In the case of rare earth metals, the contribution of both spin and orbital motion is significant for their magnetic characteristics. In addition to these elements strong magnetic properties are also showed by many compounds, metal oxide and alloys of transition metals with rare earth metals.

### 1.3.2 Types of Magnetism in Perovskites

Although various kinds of magnetic behavior such as diamagnetism, paramagnetism, ferromagnetism, antiferromagnetism and ferrimagnetism are exihibited by different magnetic materials, pervoskites show mostly antiferromagnetic, ferromagnetic some cases spin glass behavior.

**(a) Ferromagnetism**

Magnetic materials which possess the permanent magnetic moment i.e, spontaneous magnetization without the presence of any magnetic field and the magnetic ordering temperature are called ferromagnetic materials. In ferromagnetic materials all the magnetic moments are aligned along a unique direction shown in **figure. 1.5**.

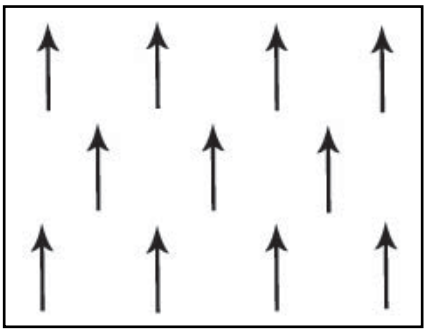

***Figure 1.5*** *Schematic diagram of magnetic dipole moments of ferromagnetic material aligned in single direction.*

Ferromagnetic behavior is found in materials e.g. nickel, cobalt and iron, due to their unfilled orbits. Mostly ferromagnetism metals have partially filled bands of 4s and 3d. The spontaneous magnetization is not manifest in magnetic materials which are not exposed to an external magnetic field. As per Weiss theory the ferromagnetic materials consist of a number of small regions which are spontaneously magnetized called domains. In the absence of magnetic field each domain magnetized its own direction. When the external magnetic field is absent the magnetization of the different domains having a different orientation and as a result the total magnetization average is zero. Under the influence of magnetic field, the magnetic domain parallel to the direction of field tends to expand more inducing magnetization. Ferromagnetic materials follow the Curie-Weiss law shown in **figure 1.6.** The temperature above which the ferromagnetic materials transform into paramagnetic called the Curie temperature, $T_C$. The susceptibility ($\chi$) of the ferromagnetic material at $T > T_C$ is given by:

$$\chi = C/(T-T_C) \qquad (1.1)$$

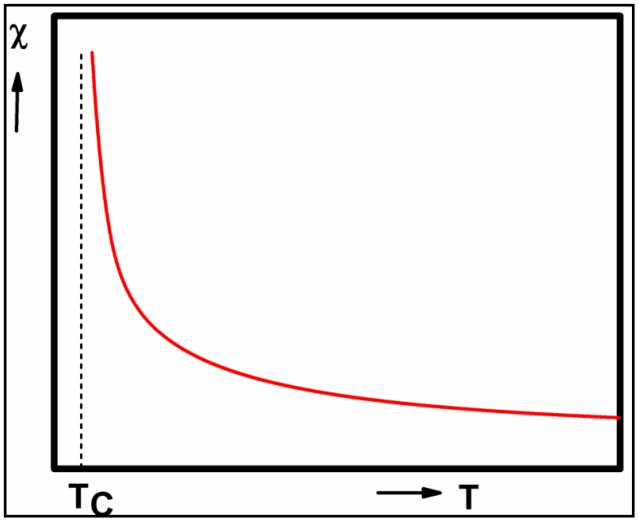


***Figure 1.6*** *Curie – Weiss Law for ferromagnetic materials.*

At T >$T_C$ the $\chi$ is positive and when *T* becomes equal to $T_C$, $\chi$ is infinite, which correlated with the order spontaneous phase [8]. This means that without the presence of external magnetic field, the ferromagnetic materials show spontaneous magnetization behavior. The graph of magnetization (*M*) versus magnetic field (*H*) shown in **figure 1.7** is known as a hysteresis loop [9]. The concept of hysteresis depends on domain. As the magnetic field increase the magnetization increases due to grow of the domain which pointing along the magnetic field direction. The growth of the domains continues until the favorable domains grow up to the maximum extent with their magnetisation called the saturation magnetisation ($M_s$). After saturation, a finite value of magnetization exists when the value of magnetic field is decreased to zero, known as the remnant magnetisation ($M_r$). To reduce the magnetisation to zero, a reversed magnetic field required is known as the coercivity ($H_c$). Such types of properties are found in ferromagnetic materials.

,

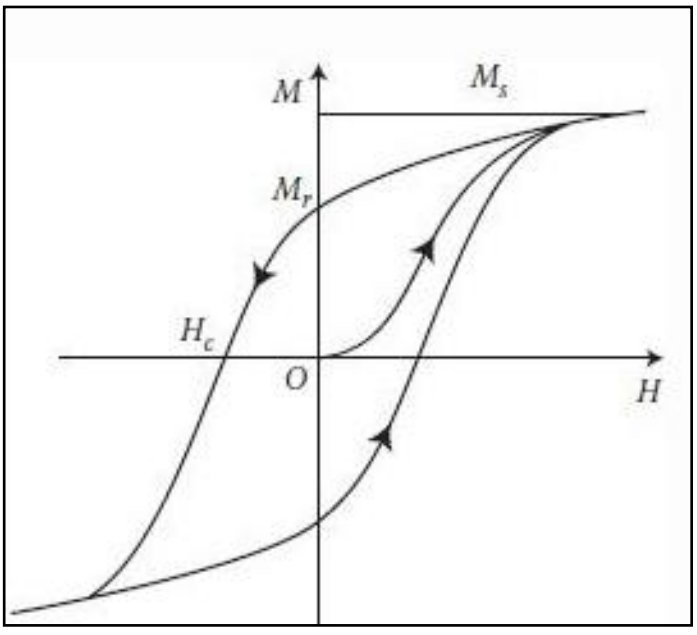


***Figure 1.7*** *Schematic plot of magnetic hysteresis loop for ferromagnetic material [9].*

**(b) Antiferromagnetism**

Antiferromagnetism originates when the magnetic moments of the neighboring atoms are arranged in opposite direction as shown in **figure 1.8.** Below Néel temperature ($T_N$), the temperature at which paramagnetic converts into antiferromagnetic, antiferromagnets are separated onto two sublattices of indistinguishable ions. The magnetic moment of the first sublattice is polarized in one direction while the magnetic moment of the second one is polarised in the reverse direction by the equal amount.

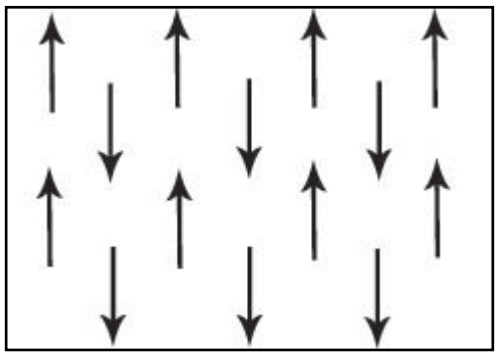

***Figure 1.8*** *Schematic diagram of magnetic dipole moment of anti- ferromagnetic material align in opposite direction.*

The spins of atoms between nearest neighbours will be antiparallel at *T=0*. Accordingly, the net magnetic moment is zero. Very often this type of magnetism occurs in system which can be considered as two interpenetrating sulattices. This type of magnetism is first observed in MnO crystal. The complication of this type of material is that there are several manners of arranging an identical number of up and down spins depending on the type of crystal lattice on which the spins are to be placed. These arrangements of spins result in different types of antiferromagnetic (AFM) ordering such as A, C and G type as shown in **figure 1.9.** In A-type the intra-plane coupling is ferromagnetic and inter-plane coupling is antiferromagnetic, while in case of C-type, intra-plane coupling is antiferromagnetic and

inter-plane coupling is ferromagnetic. In the case of G-type both intra and inter coupling is antiferromagnetic.

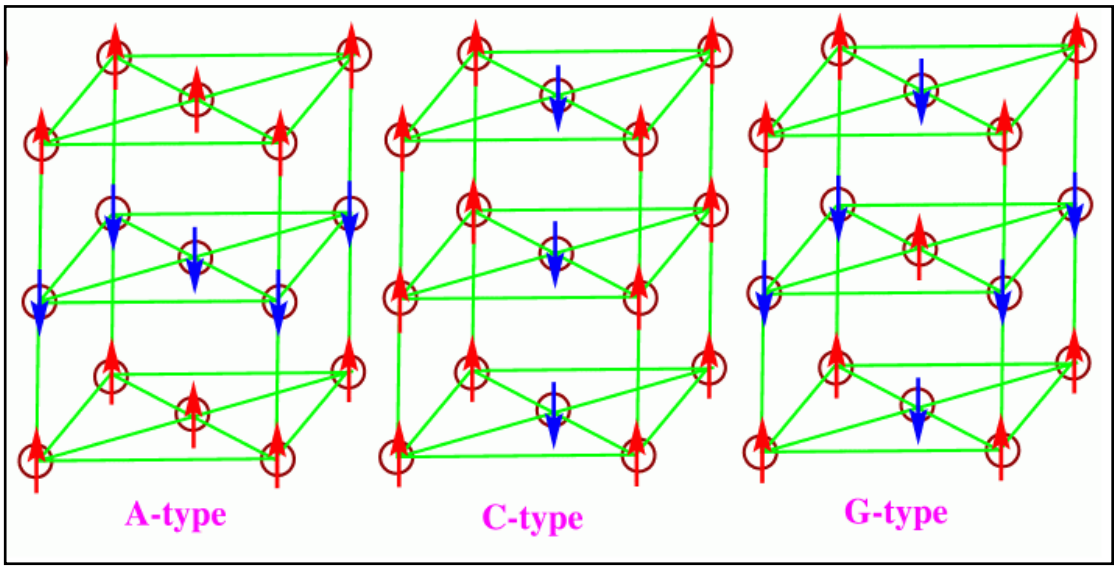


***Figure 1.9*** *Different types of antiferromagnetism.*

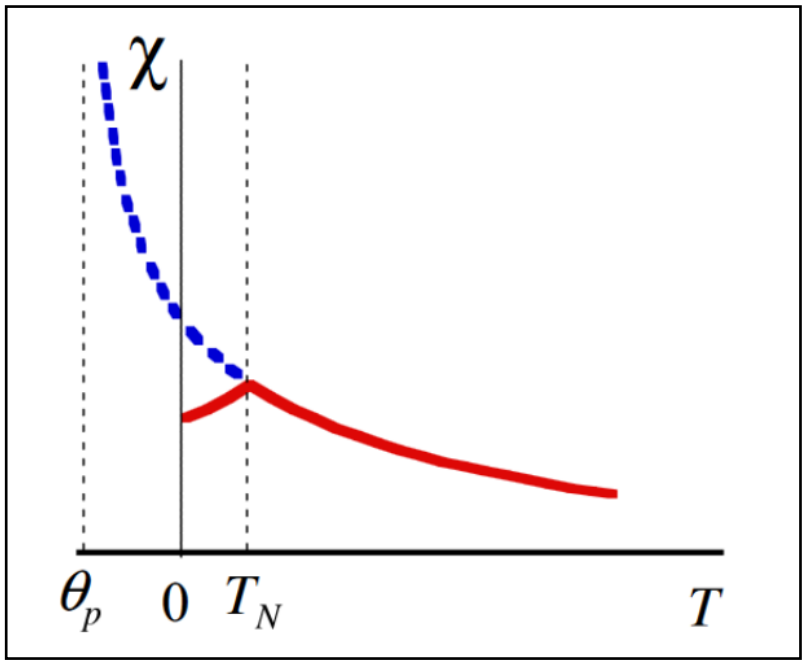


***Figure 1.10*** *Curie –Weiss law for antiferromagnetic materials [10].*

The susceptibility of antiferromagnets is temperature dependent as shown in **figure 1.10**. . The magnetization becomes maximum at a critical temperature known as the Neel temperature, $T_N$. Above $T_N$, the material become paramagnetic while below $T_N$ it behaves like a antiferromagnet. Unlike the ferromagnetic materials, the antiferromagnetic material do not show infinite susceptibily at $T=T_N$. Below the $T_N$, the susceptibility decreases slightly with decreasing temperature. The concept of antiferromagnetism is explained on the basis of molecular field theory which is developed by Neel.

**(c) Spin glass**

Spin glass is described as a random, magnetic system having the mixed interactions characterized by a random, yet cooperative, freezing of spins at a well defined temperature $T_f$ known as the freezing temperature. Below $T_f$, magnetic long-range ordering is absent with the appearance of a metastable frozen state. For example, in the alloy of CuMn in which the atomic percent of Mn is low showing both ferromagnetic and antiferromagnetic interactions. The net result is that there is frustration with no defined ground state due to compition between FM and AFM. At $T_f$ the moments get stuck due to formation of clusters as the moment slow down in low temperature. Due to the randomness, there is a distribution of distance between the spins appears and this gives the frustration and show spin glass behavior. The above magnetism are drived by the magnetic exchange interaction between the ions.

### 1.3.3 Magnetic Interactions

On the basis of interaction among the different atoms, the magnetic behavior can be determined. The magnetism of the magnetis system are explained on the basis of different exchange interactions. These interactions can be well explained using Heisenberg's

exchange integral. These interactions are separated into categories: (i) direct and (ii) indirect exchange interactions.

#### 1.3.3.1 Direct Exchange Interaction:

Exchange energy plays an important role in total energy of any molecules and the formation of co-valent bond in many solids. The exchange energy $E_{ex}$ is given by Heisenberg is [6, 8]:

$$E_{ex} = -J_{ex}\, S_i.S_j = -J_{ex}\, S_iS_j \cos\theta \qquad (1.2)$$

where the electronic spins at the i and $j^{th}$ atomic sites are represented by $S_i$ and $S_j$ , repectively which can take values +1/2 or -1/2. The exchange integral and the angle between these two spins are denoted by $J_{ex}$ and $\theta$. When the spins are parallel the value of $\cos\theta$ is 1 while it is -1 when the spins are anti parallel. Exchange integral $J_{ex}$ is positive for ferromagnetic and for anti- ferromagnetic materials it is negative. Exchange forces are responsible for ferromagnetism and antiferromagnetism in the materials. **Figure 1.11** shows the plot between the sign and magnitude of $J_{ex}$ and inter-atomic distance, is known as Bethe-Slater plot. From plot one can seen that $J_{ex}$ is positive for ferromagnetic materials and negative for antiferromagnetic materials. Such exchange interaction arises among spin on ions close enough to show enough overlap of their wave functions. The adjacent single free atoms residing beside each another that posses respective lobes of charge density are attributed to different states. Specifically, these lobes of charge produce an overlap region of charge density which is contributed to individual atoms. It results in a strong short-range coupling, which diminishes quickly on increasing the separation between the magnetic ions. In direct exchange interaction, exchange integral ($J_{ex}$) can be positive or negative depending on the basis of equilibrium between kinetic and coulombic energies. Thus, for

two atoms having single electron each, the coloumbic interaction is minimal when they are very close to one another and the electrons pay out most of their time in between the nuclei. Since the electrons are then desired to be present at the same position in space at the same time, then according to Pauli's exclusion principle, it is necessary for them to possess antiparallel spins. Due to this antiparallel alignment, AFM ordering exist and therefore negative value of exchange interaction $J_{ex}$. But, when the atoms are so far apart, the electrons pay out their time for away from each other to reduce the electron-electron coulombic interaction. This can give rise to a parallel alignment of the spins, i.e. FM ordering with positive exchange interaction. With the help of the Bethe-Slater curve as shown in **figure 1.11,** the nature of direct exchange interaction can be determined.

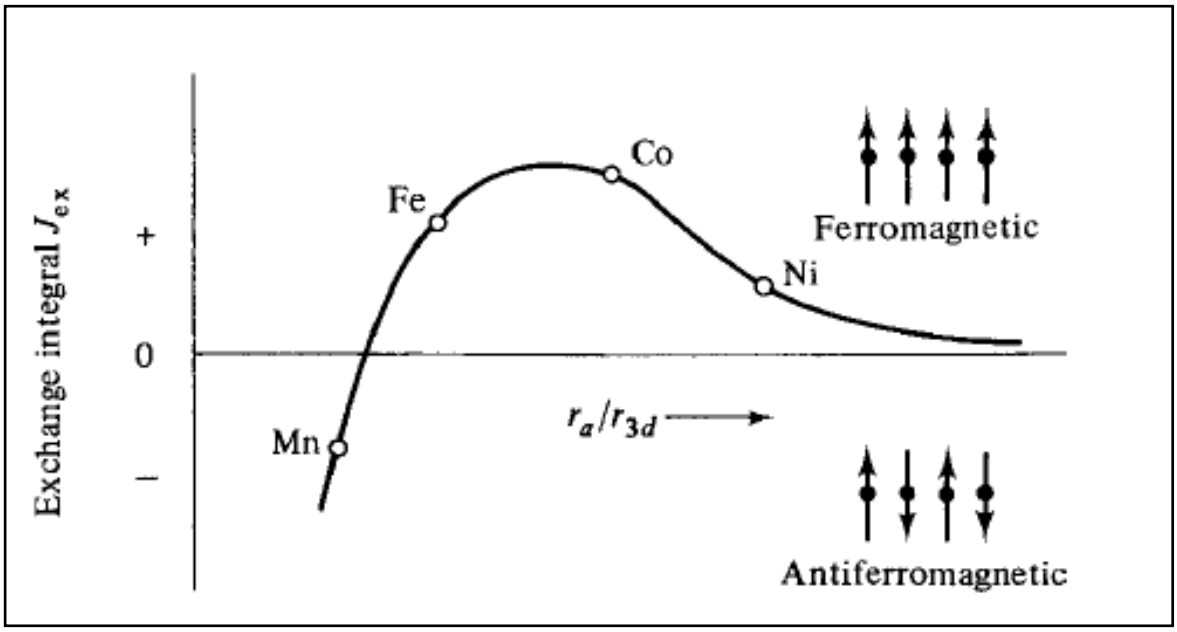


***Figure 1.11*** *Bethe–Slater curve for ferromagnetic and antiferromagnetic materials [8].*

### 1.3.3.2 Indirect Exchange Interaction

**(a) Super Exchange Interaction**

Direct exchange refers to the interaction between neighbouring moments, but in super-exchange interaction, coupling between two nearest-neighbour cations are occurred by a shared non-magnetic ion (e.g. oxygen). The transition metal oxides are a good example for the super-exchange interaction. In the case of transition metal oxides, the hybridiation occurs between the 3d-orbitals and the 2p-O orbitals. The total energy of the system decreases due to virtual hopping of O-2p electrons to the overlapping orbitals of transition metal (TM) producing different excited states. For example, taking a system having two magnetic atoms in which each atom posses a single d electron and separated through an oxygen atom. In the case of ionically bonded system, the oxygen ion with its two p-orbital electrons will overlap with the magnetic atom's d orbitals (**figure 1.12**).

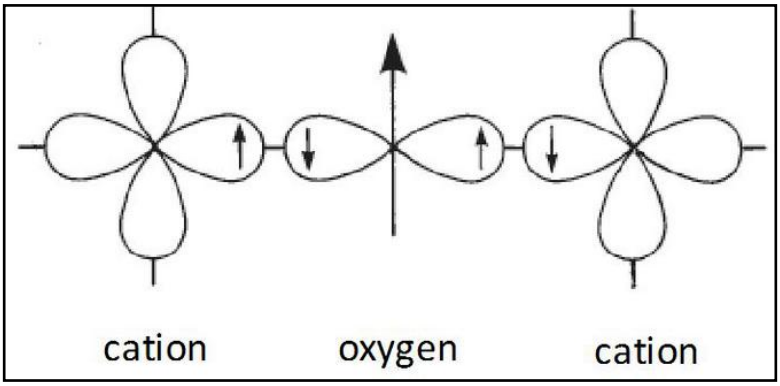


***Figure 1.12*** *Schematic representation of super-exchange interaction in magnetic oxides. The p-orbital of anion interact with d orbital of transition metal cations [11].*

When the magnetic atoms are ordered antiferromagnetically, the energy of the system is lowered because of the electrons are freely to move from the oxygen ion to either magnetic ion. The strength of the antiparallel coupling among metal ions (M) depends on the bond

angle M-O-M and it is usually highest when the value of angle is $180^{o}$ i.e. when the spins are collinear.

**(b) Double Exchange Interaction**

The double exchange interaction (DE) was given by Zener [12]. It is an indirect type of interaction that occurs between the spins of magnetic ions having mixed valence. For example, Manganese ion can occur in +3 and +4 oxidation states, i.e. as $Mn^{3+}$ and $Mn^{4+}$, in the mixed-valence manganite system such as $La_{1-x}Ba_xMnO_3$. The FM originates in such systems is governed by the double exchange (DE) mechanism and can be understood considering figure 1.13. In the case of mixed valency of Mn ions, e.g. electron on $Mn^{3+}$ ion

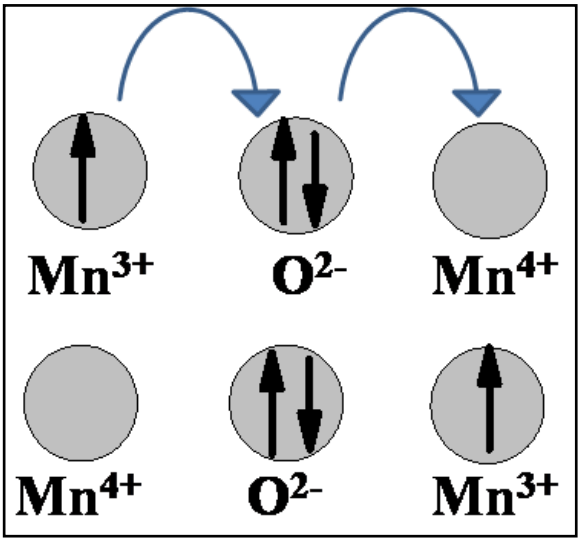


***Figure 1.13*** *Schematic diagram for double exchange interaction.*

can jump to a neighboring site of $Mn^{4+}$ via oxygen by interacting with 2p electrons of $O^{2-}$ .This is possible only if there is a vacancy of the same spin. However, due to the strong Hund's coupling, the three electrons in the $t_{2g}$ level want to keep the $e_g$ electron aligned to

them. Thus it is not energetically favorable for an $e_g$ electron to hop to an adjacent ion where the $t_{2g}$ spins will be antiparallel to the $e_g$ electron. FM arrangement of neighboring ions is required to retain the high-spin arrangement of both the receiving and the donating ions. This model is alike to superexchange. In superexchange, an AFM or an FM alignment takes place among two atoms having the same number of electrons (valence), while in double exchange; the interaction takes place only when one atom has an extra number of electrons compared to the other.

**(c) Dzyaloshinskii-Moriya (DM) Exchange Interaction**

Spin-orbit interaction plays the same role as oxygen atom in superexchange. The Dzyaloshinskii-Moriya (DM) interaction is a process, in which the excited state is not connected with oxygen as in case of superexchange interaction but is originated by the spin-orbit interaction in one of the magnetic ion. Afterwards an exchange interaction occurs between the excited state of a magnetic ion and the ground state of the neighboring ion. This type of interaction is called as Dzyaloshinskii-Moriya (DM) interaction or anisotropic exchange interaction. When this type of interaction is present between spins $S_i$ and $S_j$ it is given in the form of a new term Hamiltonian i.e.

$$\mathbf{\hat{H} = D \cdot (S_i \times S_j)} \qquad (1.3)$$

The Dzyaloshinskii- Moriya vector D is finite when there is no inversion symmetry exists in crystal field in respect of the centre between $S_i$ and $S_j$. However in general, the D can not be vanish and depending on the symmetry it will lie parallel or perpendicular to the line connecting the two spins. A weak ferromagnetism occurs in an antiferromagnetic structure due to a small canting of the moments. DM interaction is responsible for this weak ferromagnetism. It is found in $MnCo_3$, $CoCo_3$ and $Fe_2O_3$ etc [6].

## 1.4 Review of Literatures

### 1.4.1 Synthesis, Structure and Physical Properties of $GdMnO_3$

#### 1.4.1.1 Synthesis of $GdMnO_3$

$GdMnO_3$ perovskites are synthesized by using various techniques e.g. solid- state reaction, co-precipitation method, sol-gel technique, hydrothermal processing. Detailed information of synthesis methods of $GdMnO_3$ perovskite are discussed. $GdMnO_3$ can be synthesized by through standard solid- state reaction route [12-15]. For the synthesis of sample, the powders of $Gd_2O_3$ and $MnO_2$ / $Mn_3O_4$ are taken in stoichiometric proportion and then mixed it and ground well. The mixture is calcined in air at different temperatures for different time to obtain the pure phase of $GdMnO_3$. Co-precipitation is another synthesis process for the preparation of $GdMnO_3$ [16, 17]. In this synthesis, stiochiometric quantity of Gadolinium nitrate ($Gd(NO_3)_3$) and Manganese (II) nitrate ($Mn(NO_3)_2$) of high purity are taken in a beaker and dissolve it in distilled water (100 ml). Afterwards the solution is mixed homogenously with the help of magnetic stirrer for 6 hrs. To the above solution, ammonium hydroxide ($NH_4OH$) is added drop wise with constant stirring to attain the pH value >10 for complete precipitation. The precipitate is washed after filtering using distilled water for numerous times, then dried the precipitate at 100 $^oC$ using an oven for 12 hrs. As prepared precursor sample is calcined at different temperature and for different time. $GdMnO_3$ nanoparticles are prepared by the sol-gel technique [18-21]. In this method, for the preparation of sample the stoichiometric proportions of $Gd(NO_3)_3 \cdot 5H_2O$, $Mn(NO_3)_2 \cdot 5H_2O$ and citric acid are taken in a beaker with distilled water. The molar ratio of cation-to-citric acid is kept in 1:2. To obtain the viscous gel the solution is stirred at 85 $^oC$ using a magnetic stirrer. The gel is dried at 100 $^oC$ for 8 h and a fine black powder is

obtained after grinding. Finally, the black powder is calcined at different temperatures. One can also synthesize the $GdMnO_3$ by using hydrothermal technique [22]. In this method, stiochiometric amounts of ($Gd(NO_3)_3 \cdot 6H_2O$), ($Mn(NO_3)_2 \cdot xH_2O$) and equal quantity of citric acid ($C_6H_8O_7$) (metal to citric acid molar ratio is kept in1:1) are taken and dissolve in deionized water. Further, addition of ethylene glycol enhances the gelation, because it minimize the diffusion path for the metal precursors to form uniform complexes. Then the transparent solution is stirred for 6 h and ammonia solution is added drop-wise to raise the pH value of the solution ~9.2 for sol formation and again the sol is stirred for 3 h. The sol is transferred to an autoclave having Teflon liner. Under the autogenous pressure the sol is heated at 200 ºC upto 24 h. When the reaction is completed the precipitate is filtered and subsequently washed using deionized water for the removal of unreacted precursors then dried the precipitate at 120 ºC. The resulting powder sample is annealed for 6 h at 700 ºC.

#### 1.4.1.2 Structure of $GdMnO_3$

$GdMnO_3$ with distorted orthorhombic structure O' at room temperature having space group, *Pbnm* has been reported by many authors [23-25]. Distorted structure O' in $GdMnO_3$ is due to presence of J-T active element, $Mn^{3+}$ ions. Many authors have changed the O' orthorhombic structure which is more distorted, to O type orthorhombic one which is more symmetrical by doping in either Gd site or Mn site or by applying pressure [12, 21, 26-28]. In this context, Lin *et al.* have increased the structure stability by applying 50 GPa pressure in $GdMnO_3$ [29]. On the other side by doping divalent and monovalent ion in Gd site can produce $Mn^{4+}$ ions which is not J-T active also tend the structure towards more symmetrical. Nandy *et al.* have reported that the symmetry of the structure is increased by doping monovalent Na in Gd site [21]. Hirano *et al.* have also reported that the structure

stability of $GdMnO_3$ is increased after doping divalent Sr in Gd site [30]. Pal *et al.* have synthesized Fe doped $GdMnO_3$ by solid state route and increased the stability of the structure by doping Fe in Mn site [31].

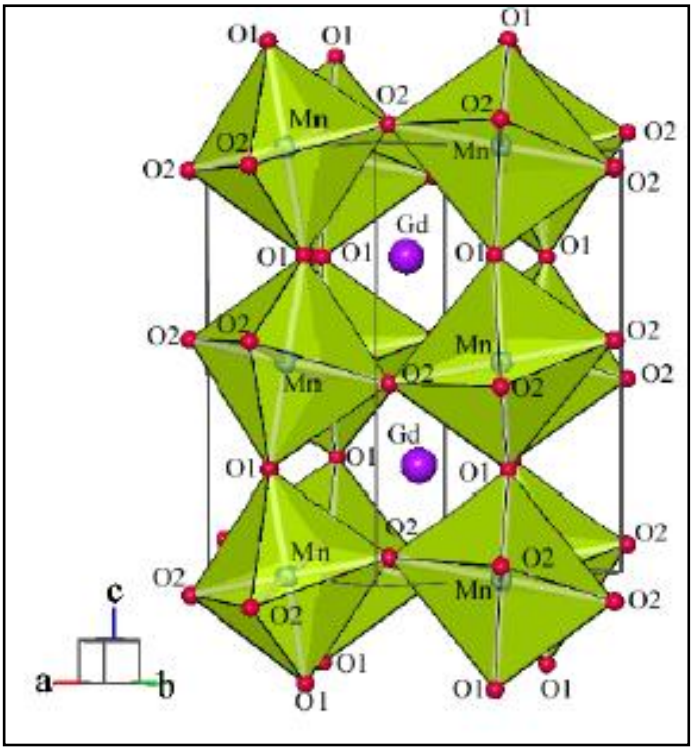


***Figure 1.14*** *Crystal structure of $GdMnO_3$ [29].*

### 1.4.1.3 Physical Properties of $GdMnO_3$

The physical properties such as magnetic, dielectric and electrical have been studied by doping either Mn or Gd site in $GdMnO_3$. In this regard many authors have studied the magnetic properties in $GdMnO_3$ after doping Fe and Cr. The magnetic properties in pristine $GdMnO_3$ reveals canted AFM at ~23 K along with $T_N$ at ~ 42 K [32]. At ~ 6 K the ordering of the $Gd^{3+}$ ions exists [22]. One can tune its magnetic properties by doping either in Gd or Mn site. In this context, Nandy *et al.* have reported that by doping monovalent Na in Gd

site, both the octahedral and lattice distortions in $GdMnO_3$ are reduced because of Na doping. Owing to Na doping decrease in bond length of Mn–O is observed which signifies the reduction in the Jahn–Teller distortion. After Na doping in $GdMnO_3$, the changes in microstructure are occurred which effect the magnetic properties of the material as the magnetic transition temperature enhances as well as the ferromagnetic interaction become stronger. The Neel temperature shifts from ~ 42 K to ~ 51 K when Na is doped in Gd site [21, 33]. Dal *et al.* have reported that magnetic properties are influenced by Jahn-Teller effect. As a result when Ba is doped in Gd site, the Neel temperature decreases from 70 to 59 K [34]. Ibarhim *et al.* have reported that when concentration of Eu exceeds from 20 atomic % in $Gd_{1-x}Eu_xMnO_3$, the structural distortion may destroy the spin arrangement which deteriorates the ferromagnetic behavior [35]. Sarguna *et al.* have repoted that ionic radius of $Y^{3+}$ (1.075 Å) is smaller than $Gd^{3+}$ (1.107 Å), decreases the bond angle of Mn–O–Mn from 146.1° to 144.69° reducing $T_N$ from ~ 34 K to ~ 32 K [26]. Same modifications can also be done by doping in Mn site. In this context, Pal *et al.* have doped Fe in Mn site and have observed that the static orbital ordering produced through the J–T distortion seems to have an significant role in altering the $T_N$ [31]. Magnetization reversal is found in $GdMnO_3$ when Sr, La and Ca are doped in Gd site [36-38]. Optical properties of the $GdMnO_3$ nanoparticles are reported by various authors. Optical absorption is measured in the wavelength range 200–600 nm at RT to find out the band gap by using Tauc's relationship [39]. Negi et al. have found a optical band gap ~ 2 · 9 eV from a plot drawn between $(\alpha hv)^{2/3}$ and photon energy ($hv$) [39]. In the case of Cr doped $GdMnO_3$, Singh et al have reported that the band gap is decreased from 4.4 to 3.7 eV [17]. Three shoulder peaks which are centered at ~ 2.0, 2.3, and 2.7 eV are observed due to electron transition of Mn

3d [40-43]. An absorption peak with higher energy centered at ~4.1 eV is obtained due to the multiple transitions of charge-transfer between the states O 2p and Mn 3d. The ultraviolet emission peaks obtained at ~ 396 and ~406 nm, while ~466 nm is due to the blue band emission and these emissions are because of the transfer transitions of spin-allowed charge [44, 45]. In the photoluminescence spectra, there are four distinct charge transfer bands produced at 3.5, 4, 8, and 8.5 eV due to the transition of electrons from O 2p→Mn($t_{2g}$ − JT), Mn($t_{2g}$ + JT), Mn($e_g$ − JT), and Mn($e_g$ + JT), respectively [46, 47]. On the other hand, $Mn^{4+}$ energy levels are realized according to Tanabe–Sugano diagram for $3d^3$ configurations in an octahedral symmetry. The spin allowed electronic transitions are observed when electrons move from higher energy states such as $2E_g$, $4T_{2g}$, $2T_{2g}$, $4T_{1g}$, etc., to ground state $4A_{2g}$ [48]. The dielectric constant of $GdMnO_3$ at 1 MHz is 83.2 which increases to $6.3 \times 10^3$ when Ba is doped in Gd site [34]. So giant dielectric properties are obtained in Ba doped $GdMnO_3$ sample. They have proposed that the origin of the high value of dielectric constant in $GdMnO_3$ with Ba doped ceramics can be related with the polar arrangement of the electrons of mixed valancy of $Mn^{3+}$/ $Mn^{4+}$. Singh *et al.* have shown that the dielectric constant ($\varepsilon_r$) is found to be higher than $GdMnO_3$ at all temperatures and frequencies when Cr is doped at Mn site. Interstitial sites of $GdMnO_3$ have been incorporated by the Cr ions. Due to these interstitial sites transfer of atoms become easier in comparison to perfect lattice, as a result the domain motion occur caused by small electrical fields and increases the dielectric constant [17].

### 1.4.2 Synthesis, Structure and Physical Properties of $LaMnO_3$

#### 1.4.2.1 Synthesis of $LaMnO_3$

$LaMnO_3$ perovskites are synthesized by using various techniques e.g. sol-gel technique, hydrothermal processing and sono-chemical method. Detailed information of synthesis method of $LaMnO_3$ perovskite are discussed here.

In sol-gel method, for the preparation of sample 0.1M of both $La(NO_3)_3.6H_2O$ and $Mn(NO_3)_2.4H_2O$ are dissolved separately in distilled water. After that these two mixtures are added to stearic acid (0.4M) and for the formation of a dark homogeneous mixture stirred it with the help of magnetic stirrer. A homogeneous sol is prepared when the mixture is heated at 120 ºC for 3 h in an oven. The sol is cooled to RT and a gel is obtained when it is dried at 400 ° C for 12 hours in an oven. Finally, the obtained gel is calcined for 2 h at 800 ° C for the formation of pure $LaMnO_3$ nanoparticles [49]. For the preparation of $LaMnO_3$ by sono chemical method, 0.1 M $La(NO_3)_3.6H_2O$ and 0. 1M $C_6H_9MnO_6.2H_2O$ are taken in a beaker. A solvent like decalin which is having the low volatility is added in small amount to the reactant mixture to enhance the power transfer of the system. SDS surfactant is added to reduce the agglomeration. For sonication, direct immersion of Ti horn (1500 W, 20 kHz, Vibracell, USA) is placed into the solution at RT for 2 h. During the sonication, oxalic acid is added in solution. For the complete precipitation, sonication is continued for 4 h. After that the precipitate is washed with acetone and alcohol. Then the powder is dried under vacuum at 40 ºC. Finally the powder is calcined for 2–10 h in the temperature range 700–800 ºC [50] .

In hydrothermal synthesis method, first 5 mole of $La(NO_3)_3 \cdot 6H_2O$ and $Mn(NO_3)_3$ solution are added in distilled water. Then stirred the solution for mixing and add the KOH dropwise for precipitatation. Due to the addition of KOH, a white precipitate is appeared instantly. The precipitate is transferred into the deionzed water filled autocalve ( upto 80% water) after stirring 10 min. Then sealed it and for about 12h heated it at $180^o$ C. After the reaction and cooling down to RT the final product of brown powder is produced which is collected after washing with deionized water and then dried it at 60 $^oC$ in air. To obtain $LaMnO_3$ oxides, it is calcined at 600-$900^o$ C for 3h [51].

#### 1.4.2.2 Structure of $LaMnO_3$

$LaMnO_3$ crystallizes in the many structure such as rhombohrdral and orthorhombic perovskite structure with space group R-3c and *Pbnm* ,respectively [52, 53]. Many authors tune its crystal structure by doping in either La site or Mn site. In this context, Nagabhushana *et al.* have reported that undoped $LaMnO_3$ nanocrystalline powder rhombohedral structure converts into cubic phase when Ba is doped [54] while Nam *et al* have reported that it transforms into pseudocubic when Sr is doped in La site [55]. Deisenhofer *et al.* have found that when Cr is doped in La site upto 0.3, it shows O' orthorhombic which converts into psudocubic one when the concentration lie between $0.3<x<0.4$ [56]. Das *et al.* have reported the orthorhombic structure when Ce is doped in La site [57]. Gonen *et al.* have reported that when Li is doped in Mn site, rhombohedral structure is found [58]. Hebert *et al.* have reported that with increasing the concerntration of Ga in Mn site, the distortion in cell reduces only smoothly having the O' orthorhombic structure reflecting a cooperative J-T effect. Conversely, when the Ni is substituted, a large development in the cell parameters is found. When $x > 0.15$ the distortion reduces very

quickly and the structure transform from O' to *O*-type orthorhombic which indicates that the J-T distortion has vanished. In the case of Li substitution, the result is more dramatic, with increasing concentration as a structural transition is found from orthorhombic to rhombohedral [59]. Besides this, La and Mn vacancies also establish the existence of a pseudocubic crystallographic phase. Ritter et al. show that La vacancy is accompanied with oxygen rich composition display three different crystal structures such as orthorhombic with large J-T distortion, orthorhombic with small J-T distortion and rhombohedral structure [60].

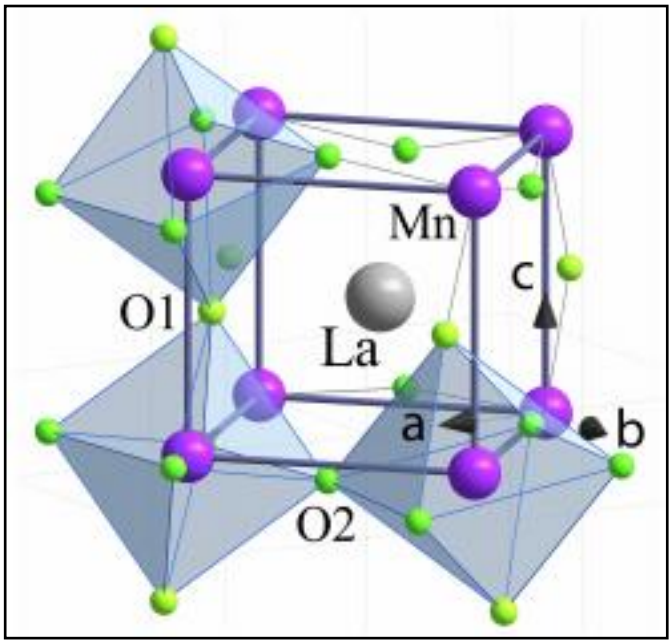


***Figure 1.15*** *Crystal structure of $LaMnO_3$ [61].*

### 1.4.2.3 Physical Properties of $LaMnO_3$

Basically $LaMnO_3$ shows antiferromagnetic property with $T_N$ ~ 140 K [62-64]. The J-T distortion, namely, the modulation in the Mn-O bond lengths, strongly correlates with the magnetic structure and the lattice constants. As per the tight binding approximation, *W*

i.e, the electronic band width depends on the bond angle Mn–O–Mn ($\varphi$) and bond lengths Mn–O and can be expressed as $W = \cos \omega$/Mn–O, where $\omega$ *is* the tilt angle and defind as $\omega=(\pi-\varphi)$. It has been reported in literature that $T_C$ is different for different structure of $LaMnO_3$. For example, Hernandez et al. observe the $T_C$ at 150 K in hexagonal $LaMnO_3$ [16], Brankovic *et al.* report $T_C$ at 180 K in rhombohedral structure [20] and Ghosh *et al.* observe at 120 K for orthorhombic one [15]. While monoclinic phase with higher J-T distortion than the rhombohedral structure is reported by Ghosh *et al*. [15]. Brankovic´ *et al.* have found that when Sr and Ca are doped in La site the distortion is less as a result, $T_C$ increases [65]. In the case of Ni doped $LaMnO_3$, the Neel temperature increases from 140 to 150 K when Ni increase to 20 at% and O' structure converts into O type orthorhombic structure [59]. Das *et al.* have reported that when Ce is doped in La site, $T_C$ is increased upto x=0.3 and when $x>0.4$, $T_C$ remains almost unchanged. After the doping level $x>0.4$, segregation of Ce may be the possible reason for this behavior [57]. De *et al* have found that when Fe is doped in Mn site the $T_C$ is decreased from 140 to 132 K when x increases from 0 to 0.15 [66]. In addition, a crossover from antiferromagnetic, orthorhombic structure to ferromagnetic, rhombohedral structure have been reported under oxygen rich condition [60].

### 1.4.3 Magnetization Reversal in Perovskites

Magnetization reversal (MR) is a phenomenon which occurred in a material when dc magnetization a function of temperature, crossover from positive to negative value when the temperature is lowered from its magnetic ordering (**figure 1.15)** . Several magnetically ordered materials e.g. perovskites, spinel ferrites, intermetallic alloys, multilayers, molecular magnets and garnets have shown the MR phenomena experimentally[67]. This

phenomenon is governed by various intrinsic parameters, e.g. magnetic anisotropy, crystal structure, temperature dependence of sublattice magnetization and magnetic exchange interactions. The mechanism behind the MR depends on negative exchange coupling among following types of sublattices.

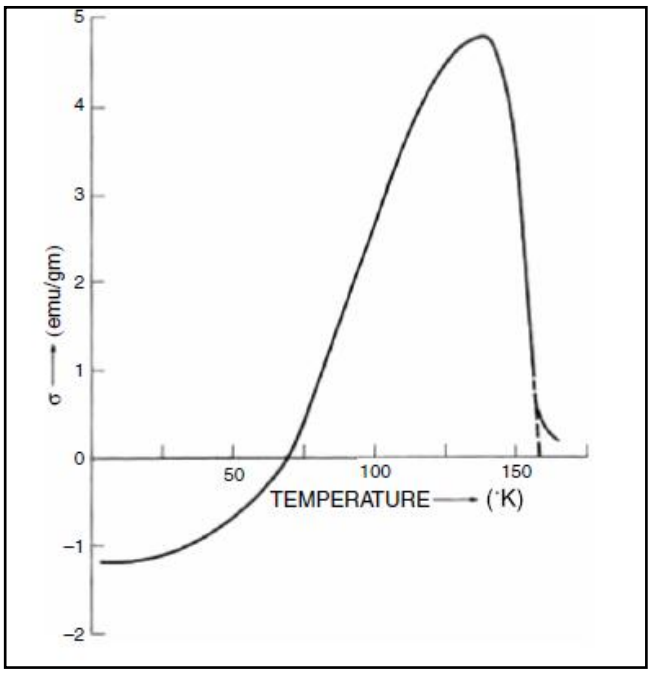


***Figure 1.16*** *Schematic diagram of negative magnetization [68].*

**(a) Ferromagnetic (FM) sublattices:** Negative exchange coupling between FM sublattices are found in ferrites ($AB_2O_4$) and inverse ferrites are observed because a antiparallel ordering which corresponds to different crystallographic sites occurs between two (or more) FM sublattices. For example in case of $Co_2VO_4$ having inverse spinel (fcc) structure, MR occurs due to the antiparallel moments of $Co^{2+}$ (A site) and $Co^{2+}/V^{4+}$ (B site) having different temperature dependences as per Néel's theory [68]. The other examples are $Fe_2MoO_4$ [69], $NiFe_{1.33}V_{0.67}O_4$ [70], $CoCr_{2-x}Fe_xO_4$ ($0.1 \leq x \leq 0.22$) [71, 72], and

$FeCr_{2-x}Al_xS_4$ [73] in which the magnetization reversal phenomenon are present due to negative exchange coupling.

**(b) Canted antiferromagnetic (c-AFM) sublattices:** Negative exchange coupling between c-AFM sublattices is the other reason of presence the MR. In this there is an antiparallel ordering occurs between c- AFM sublattices belong to different crystallographic sites. Many perovskites such as $RVO_3$ have discussed the negative magnetization related to this category. The other examples which are correlated to this category are $La_{1-x}Ca_xCoO_{3-\delta}$ ($0.5 \leq x \leq 0.6$) [74], $CaMn_{0.96}V_{0.04}O_3$ [75], $CaMn_{1-x}Fe_xO_3$ (x = 0.08, 0.1) [75], and $CaMn_{1-x}Sb_xO_3$ (x = 0.05, 0.08) [76, 77].

**(c) FM/canted AFM and paramagnetic(PM) sublattices**: In many system the presence of negative magnetization is discussed on the basis of an antiparallel coupling between FM/ canted AFM and PM sublattices residing at different crystallographic sites. For example in the case of $La_{1-x}Gd_xMnO_3$ (x = 0.25, 0.5, and 0.75) the MR is present due to the magnetism originates from complex interplay of the 3d–4f [37].

## 1.5 Objectives

Owing to the role of orthorhombic phase transformation from O' to O type with the decrease in J-T distortion strongly correlates with their physical properties. Due to their fascinating fundamental physics and potential application in the field of multiferrocity, these materials have received a lot of attention within research communities. By incorporating dopants in rare earth site many authors are tuned their structure and magnetic properties. However, less studies focus on dopants in Mn site of perovskites. Therefore, it is of interest to study the replacement of J-T active element, Mn with non J-T active element and study the correlation of structure, microstructure, magnetic and

photoluminescence properties in pristine $RMnO_3$ (R= La,Gd) pervoskites. Details studies on Fe/Cr doped in $GdMnO_3$ and cation deficient $LaMnO_3$ pervoskites are incorporated in the thesis as the following chapters:

- Chapter 1 accounts for the introduction and literatures survey on regarding the aspects on which have been studied in this thesis work. In chapter 2, we have studied the synthesis and experimental techniques adapted to synthesize and characterize the materials.
- In chapter 3, we have discussed the sol-gel technique to synthesize $GdMn_{1-x}Fe_xO_3$ (x= 0, 0.1 and 0.2) perovskite and studied its structure, microstructure along with J-T distortion through XRD and Raman spectroscopy. Further, the magnetic properties where magnetization vs temperature, magnetization vs magnetic field and frequency dependent ac susceptibility measurements are carried out.
- In chapter 4, we have demonstrated the structural transformation with the reduction in Jahn-Teller distortion in $GdMn_{1-x}Fe_xO_3$ (x= 0.3 and 0.5) perovskites. The reduction in Jahn-Teller distortion is also correlated with the Raman and photoluminescence spectra. The surface morphology and oxygen vacancies are determined through SEM and XPS. Magnetic properties are evaluated from magnetization versus temperature, magnetization versus field measurements, remanent magnetization and frequency dependent ac susceptibility.
- In chapter 5, the effects of Cr in $GdMnO_3$ perovskite have been studied. Structural transformation optical properties, J-T distortion are evaluated using XRD and photoluminescence and Raman spectraoscopy. Magnetic reversal properties of the samples are evaluated by magnetization versus temperature measurement. Magnetic

switching properties are shown by using magnetization vs time measurement. The spin glass behavior is confirmed through remanent magnetization measurement.

- In chapter 6, we have discussed the effect of cation deficiency on structure and magnetic properties. We evaluated the reduction in J-T distortion obtained from the Rietveld refinement. The morphology of the samples are discussed by SEM. Magnetic properties are evaluated by using magnetization vs temperature and magnetic field measurement, ac susceptibility measurement. using phenomenological model. The structure and magnetic behavior is discussed on the basis of oxygen vacancies.